

5-1-2009

Retrieval of Target Photorecombination Cross Sections from High-Order Harmonics Generated in a Macroscopic Medium

Cheng Jin

Anh-Thu Le

Missouri University of Science and Technology, lea@mst.edu

C. D. Lin

Follow this and additional works at: http://scholarsmine.mst.edu/phys_facwork



Part of the [Physics Commons](#)

Recommended Citation

C. Jin et al., "Retrieval of Target Photorecombination Cross Sections from High-Order Harmonics Generated in a Macroscopic Medium," *Physical Review A - Atomic, Molecular, and Optical Physics*, vol. 79, no. 5, American Physical Society (APS), May 2009. The definitive version is available at <https://doi.org/10.1103/PhysRevA.79.053413>

This Article - Journal is brought to you for free and open access by Scholars' Mine. It has been accepted for inclusion in Physics Faculty Research & Creative Works by an authorized administrator of Scholars' Mine. This work is protected by U. S. Copyright Law. Unauthorized use including reproduction for redistribution requires the permission of the copyright holder. For more information, please contact scholarsmine@mst.edu.

Retrieval of target photorecombination cross sections from high-order harmonics generated in a macroscopic medium

Cheng Jin,^{1,2} Anh-Thu Le,¹ and C. D. Lin¹

¹*J. R. Macdonald Laboratory, Physics Department, Kansas State University, Manhattan, Kansas 66506-2604, USA*

²*College of Physics and Electronic Engineering, Northwest Normal University, Lanzhou, Gansu 730070, People's Republic of China*

(Received 7 April 2009; published 15 May 2009)

We investigate high-order harmonic generation (HHG) in a thin macroscopic medium by solving Maxwell's equation using microscopic single-atom induced dipole moment calculated from the recently developed quantitative rescattering (QRS) theory. We show that macroscopic HHG yields calculated from QRS compared well with those obtained from solving the single-atom time-dependent Schrödinger equation but with great saving of computer time. We also show that macroscopic HHG can be expressed as a product of a "macroscopic wave packet" and the photorecombination cross section of the target gas. The latter enables us to extract target structure from the experimentally measured HHG spectra, thus paves the way to use few-cycle infrared lasers for time-resolved chemical imaging of transient molecules with few-femtosecond temporal resolution.

DOI: [10.1103/PhysRevA.79.053413](https://doi.org/10.1103/PhysRevA.79.053413)

PACS number(s): 33.80.Rv, 42.65.Ky, 31.70.Hq, 42.30.Tz

I. INTRODUCTION

In recent years high-order harmonic generation (HHG) by a strong infrared (ir) laser field interacting with a gas of atoms has been widely used for the production of subfemtosecond pulses in the extreme ultraviolet (xuv) radiation [1–3]. Attosecond pulses synthesized from these harmonics are now available in several laboratories either as a single subfemtosecond burst or as trains of attosecond pulses [4,5]. The success of generating these attosecond pulses owes much to the experimental and theoretical studies of the properties of harmonics in the last two decades [6–17], especially in terms of their temporal and spatial coherences.

The physical origin of the harmonic emission in a single atom can be easily described by a three-step model [18,19]. First, at a certain initial time the electron wave packet tunnels through the potential barrier formed by the combined atomic and laser fields. Next, it propagates in the laser field and gains kinetic energy. Finally, this energy is converted into high-energy HHG photons through the recombination with the parent ion. Since the laser field interacts with a macroscopic number of atoms, a full description of experimentally observed HHG spectra requires not only the theoretical treatment of the microscopic nonlinear laser-atom interaction but also the macroscopic propagation of the radiation through the nonlinear optical medium.

Theoretically the strong oscillating laser field induces a time-dependent dipole for each atom. This induced dipole moment can be calculated quantum mechanically by solving the time-dependent Schrödinger equation (TDSE) directly. Alternatively, the induced dipole moment can also be calculated using the strong field approximation (SFA) [19]. Since HHG is generated by a focused laser beam over all the atoms in a macroscopic medium, the induced dipole moment on each atom should be inserted as a source term in the propagation equations of the harmonic field to obtain the macroscopic response of the excited nonlinear medium. Thus a typical HHG calculation consists of two parts: first, the calculation of single-atom response; second, the propagation of Maxwell's wave equation.

The most accurate way to obtain microscopic response is the numerical solution of the TDSE for the atom interacting with the laser field. Since this approach is quite time consuming because calculations need to be carried out for hundreds of peak laser intensities to account for the nonuniform laser intensity distributions inside a focused laser beam, the induced dipole moment for each atom is often calculated using the SFA. Thus except for a few rare cases, theoretical investigations of the macroscopic propagation effect for HHG are commonly carried out using SFA-calculated single-atom induced dipole moment. Despite this limitation, the temporal and spatial properties of HHG observed experimentally have been reasonably understood, especially the synchronization of the harmonics and the temporal profiles of the synthesized attosecond pulses. On the other hand, in a few examples, macroscopic HHG spectra obtained using TDSE-calculated single-atom induced dipole moments do show significant quantitative discrepancy compared to SFA-calculated counterpart [20].

The limitation of SFA for the description of single-atom response is well known [19]. Since TDSE calculation for single-atom response for feeding the macroscopic propagation equations is very time consuming, alternative accurate theoretical approach is desirable. Recently we have proposed a quantitative rescattering (QRS) theory for the calculation of HHG spectra generated by a single atom or molecule [21–23]. According to the QRS, single-atom or single-molecule induced dipole moment by the laser field can be expressed as the product of a complex returning electron wave packet and the complex recombination dipole moment between the laser-free electrons and the target ion. Furthermore, the electron wave packet can be calculated from the SFA. Since the recombination dipole moment (or photoionization dipole moment) is much easier to calculate, single-atom HHG spectra calculated using the QRS are about as fast as the SFA but a factor of thousands faster than the TDSE calculation. The accuracy of the QRS has been carefully tested against single-atom HHG spectra obtained from the TDSE. It has now been well documented that the QRS results are nearly as accurate as those obtained from TDSE

whenever accurate results from the latter can be obtained, i.e., including atoms in the single active electron (SAE) approximation and the H_2^+ molecular ion [23].

The goals of this paper are twofold. First, we want to show that macroscopic HHG spectra calculated using QRS-based single-atom induced dipole moments are nearly as accurate as those from TDSE based and are much better than SFA based. Thus we suggest that QRS be used to generate single-atom response in the macroscopic propagation equation in the future. The second goal of this paper is to show that HHG yield after macroscopic propagation can be expressed as the product of a “macroscopic wave packet” (MWP) and the single-atom recombination dipole moment. The second goal is essential if one wishes to extract laser-independent target structural information from the experimental HHG spectra.

While the first goal is quite relevant for understanding the role of the target for attosecond pulse generation, the second goal is essential if one wishes to use HHG as a tool for ultrafast dynamic chemical imaging [24,25]. Considering a typical pump-probe arrangement, a pump pulse is used to initiate a chemical reaction. The time evolution of the resulting transient molecule can be probed with another laser pulse to generate HHG at different time delays. If one can extract the structure of the molecule from the measured HHG spectra at each time delay, then the dynamic evolution of the transient molecule can be retrieved. Since ir lasers of a few femtoseconds are widely available already, this points out the potential of using ir laser pulses for dynamic chemical imaging. For such a purpose, the retrieval algorithm would be much simpler if laser-independent transition dipole moments can be extracted from HHG spectra. Many experiments of this type have emerged in recent years [26–30] where a pump beam was used to align molecules and then HHG spectra were recorded at later times. Interpretations of these experiments so far rely on simple models where macroscopic propagation effect was not considered. In view of the well-known important role of macroscopic propagation on HHG spectra generated from atoms, the neglect of propagation effect for HHG from molecules is not well founded [31]. In this paper we wish to establish whether single-atom transition dipole moments can be extracted directly from the macroscopic HHG spectra.

In this paper we will examine these two issues for rare-gas atoms since only in atomic gases we can perform TDSE calculations to benchmark our QRS model. To make this paper self-contained, in Sec. II we describe approximations used for the macroscopic propagation equations. We then summarize SFA and QRS model for single-atom response and define what so-called “MWP” is. In Sec. III we compare HHG after macroscopic propagation, both in the yields and the phases of the harmonics, using single-atom response calculated using QRS vs TDSE, respectively. We then show that we can indeed extract MWP from the propagated HHG spectra and that the MWPs are independent of the target gas if the same laser pulse and focusing condition are used. The usefulness of the present results will be elaborated further in Sec. IV. Atomic units are used throughout this paper unless otherwise stated.

II. THEORETICAL METHOD

The calculation of high harmonic generation in a macroscopic medium by an intense laser usually contains two components: (i) a single-atom theory that describes the response of an atom to the driving fundamental laser field and (ii) a propagation theory that gives macroscopic response to the medium. We describe each issue separately below.

A. Propagation equations

In our simulation, first we assume that there is no ionization effect of the medium on the fundamental laser field. In other words, the fundamental field is assumed to propagate in free space. However, ionization effect is included in the single-atom response and in the nonlinear polarization term for the harmonics. The propagation of harmonic field in the ionizing medium is described by the equation [32]

$$\nabla^2 E_h(r, z, t) - \frac{1}{c^2} \frac{\partial^2 E_h(r, z, t)}{\partial t^2} = \mu_0 \frac{\partial^2 P_{nl}(r, z, t)}{\partial t^2}, \quad (1)$$

where

$$P_{nl}(r, z, t) = [n_0 - n_e(r, z, t)]x(r, z, t), \quad (2)$$

$$n_e(t) = n_0 \left\{ 1 - \exp \left[- \int_{-\infty}^t w(\tau) d\tau \right] \right\}, \quad (3)$$

$P_{nl}(r, z, t)$ is the nonlinear polarization generated by the medium, n_0 is the neutral atom density, $n_e(r, z, t)$ is free-electron density, and $w(\tau)$ is tunnel ionization rate which can be calculated from the Ammosov-Delone-Krainov (ADK) theory [33,34]. The induced dipole moment $x(r, z, t)$ is calculated for atoms inside the medium under the fundamental laser field, which gives the atomic response to the entire laser pulse. This is called the nonadiabatic approach. We assume that the effects of absorption and free-electron dispersion are negligible. By transforming to a moving coordinate frame ($z' = z$ and $t' = t - z/c$) and employing the paraxial approximation (i.e., neglecting $\partial^2 E_h / \partial z'^2$), we obtain

$$\nabla_{\perp}^2 E_h(r, z', t') - \frac{2}{c} \frac{\partial^2 E_h(r, z', t')}{\partial z' \partial t'} = \mu_0 \frac{\partial^2 P_{nl}(r, z', t')}{\partial t'^2}. \quad (4)$$

The temporal derivative in the above equation can be eliminated by Fourier transform, yielding

$$\nabla_{\perp}^2 \tilde{E}_h(r, z', \omega) - \frac{2i\omega}{c} \frac{\partial \tilde{E}_h(r, z', \omega)}{\partial z'} = -\mu_0 \omega^2 \tilde{P}_{nl}(r, z', \omega), \quad (5)$$

where

$$\tilde{E}_h(r, z', \omega) = \hat{F}[E_h(r, z', t')] \quad (6)$$

and

$$\tilde{P}_{nl}(r, z', \omega) = \hat{F}[P_{nl}(r, z', t')]. \quad (7)$$

Here \hat{F} is the Fourier transform operator acting on the temporal coordinate. Once the harmonic field at the exit face of

the medium ($z' = z_{out}$) is computed, the power spectrum of the harmonics is obtained by integrating over the transverse direction,

$$S_h(\omega) \propto \int_0^\infty |\tilde{E}_h(r, z', \omega)|^2 2\pi r dr. \quad (8)$$

B. Fundamental laser field and geometric phase

We assume that the fundamental laser field is not modified as it propagates through the medium. In the moving coordinate frame it can be written as

$$E_1(r, z', t') = \text{Re}[\varepsilon(r, z')A(r, z', t')e^{-i(\omega_0 t' + \varphi_{CE})}], \quad (9)$$

where

$$\varepsilon(r, z') = \frac{b\varepsilon_0}{b + 2iz'} \exp\left(-\frac{kr^2}{b + 2iz'}\right) = |\varepsilon(r, z')|e^{i\varphi_{laser}(r, z')}, \quad (10)$$

$$\varphi_{laser}(r, z') = -\tan^{-1}\left(\frac{2z'}{b}\right) + \frac{2kr^2z'}{b^2 + 4z'^2}, \quad (11)$$

and

$$A(r, z', t') = \cos^2\left\{\frac{\pi[t' - \varphi_{laser}(r, z')/\omega_0]}{\tau_p}\right\}, \quad (12)$$

where $\varepsilon(r, z')$ is a Gaussian beam, ε_0 is the peak laser field at the focus, ω_0 is the central frequency, $k = \omega_0/c$ is the wave vector, and b is the confocal parameter (depth of focus) given by twice the distance along z axis for the beam to expand from its minimum cross sectional area at $z' = 0$ to twice this area. Geometric phase due to defocusing is given by φ_{laser} and $\tan^{-1}(\frac{2z'}{b})$ is the *Gouy phase*, which results in a phase shift of π relative to a plane wave as the laser passes through the focus from the far field on one side to the far field on the other side of the focus. Carrier envelope phase is represented by φ_{CE} , and τ_p in the envelope function $A(r, z', t')$ is the total duration of the laser pulse, which equals 2.75 times the full width at half maximum (FWHM) of the laser's intensity.

Let

$$t'' = t' - \varphi_{laser}(r, z')/\omega_0, \quad (13)$$

then

$$E_1(r, z', t'') = |\varepsilon(r, z')|\cos^2\left(\frac{\pi t''}{\tau_p}\right)\cos(\omega_0 t'' + \varphi_{CE}). \quad (14)$$

In order to solve Eq. (5), the nonlinear polarization of Eq. (7) in the moving coordinate frame needs to be calculated. First we compute $P_{nl}(r, z', t'')$ since in the time frame t'' the spatial component and temporal part are separated. In other words, the fundamental laser field only depends on the peak field $|\varepsilon(r, z')|$. Using the Fourier transformation, we then obtain

$$\begin{aligned} \tilde{P}_{nl}(r, z', \omega) &= \hat{F}[P_{nl}(r, z', t'')] \\ &= \hat{F}[P_{nl}(r, z', t'')]e^{-i(\omega/\omega_0)\varphi_{laser}(r, z')}. \end{aligned} \quad (15)$$

From the expression above, it can be seen that there are two contributions to the phase of the nonlinear polarization: the first one is atomic phase, which depends only on the laser peak intensity; the second is geometric phase multiplied by the harmonic order. It is known that the most time-consuming job is the calculation of the spatial dependent nonlinear polarization for atoms inside the medium as the harmonic field is propagated. It is the separation of atomic phase and geometric phase that allows one to simplify the calculation. Using a batch of laser peak intensities, the nonlinear polarizations in the time frame t'' are calculated and then stored. When it comes to solve the propagation equations for each value of ω , the nonlinear polarization in t'' for atoms inside the medium is obtained by interpolation. Meanwhile the geometric phase is added up in order to transform the nonlinear polarization to the moving coordinate frame. The use of interpolation method greatly improves the efficiency of harmonic field propagation.

C. Single atom response theory

Single atom response to a time-varying laser field, polarization, and carrier phase usually is described in the framework of the SAE approximation. In principle, one can calculate the induced atomic polarization or dipole acceleration by numerically solving the TDSE, which can then be inserted as a source term in the propagation equation. Besides the TDSE, few approaches are available. In this paper we will focus on two approaches: one is the SFA (or the Lewenstein model); the other is the recently developed QRS theory.

1. SFA

In Ref. [19] a semiclassical theory was proposed with the following assumptions: (i) all the bound states in the atom are neglected except for the ground state; (ii) in the continuum, the electron is treated as a free particle moving in the laser's electric field without the influence of the target potential. In such a strong field approximation, the induced dipole moment in the time domain is calculated from the integral,

$$\begin{aligned} x(t) &= i \int_{-\infty}^{\infty} d\tau \left(\frac{\pi}{\epsilon + i\tau/2}\right)^{3/2} d^*[p_{st}(t, \tau) + A(t)]a^*(t) \\ &\quad \times e^{-iS_{st}(t, \tau)} d[p_{st}(t, \tau) + A(t - \tau)] \\ &\quad \times E_1(t - \tau)a(t - \tau) + \text{c.c.}, \end{aligned} \quad (16)$$

where $E_1(t)$ is the electric field of the laser pulse described by Eq. (14), $A(t)$ is the vector potential, ϵ is a positive regularization constant, and p_{st} and S_{st} are the stationary values of the momentum and the quasiclassical action, respectively. In the equation, $a(t) = \exp[-\frac{1}{2}\int_{-\infty}^t w(\tau)d\tau]$ is the ground state amplitude, with the ionization rate $w(\tau)$ calculated by the ADK theory [33,34] and d is the field-free dipole transition matrix element between ground state and the continuum state. The stationary value of the momentum is given by

$$p_{st}(t, \tau) = -\frac{1}{\tau} \int_{t-\tau}^t dt'' A(t''), \quad (17)$$

and the corresponding stationary action is

$$S_{st}(t, \tau) = \int_{t-\tau}^t dt'' \left\{ \frac{1}{2} [p_{st} + A(t'')]^2 + I_p \right\}. \quad (18)$$

For hydrogenlike atoms, dipole matrix element for transition from the ground state to the continuum state characterized by a momentum p is given by

$$d(p) = i \frac{2^{7/2} (2I_p)^{5/4}}{\pi} \frac{p}{(p^2 + 2I_p)^3}, \quad (19)$$

where I_p is the ionization potential of the atom. For a non-hydrogenic atom we obtain the ground state wave function from the Gaussian code. Since in Lewenstein model the continuum state is given by a plane wave, the transition dipole matrix elements $d(p)$ of a real atom can be calculated straightforwardly.

2. QRS theory

The prediction of the Lewenstein model is known to be relatively successful for harmonics near the cutoff and not accurate for harmonics in the lower plateau region. While HHG calculated from solving TDSE is accurate in principle, it can be reasonably done only for atomic targets within the SAE approximation. Moreover, for macroscopic propagation, single-atom induced dipole moments have to be calculated for hundreds of peak laser intensities covering the interaction volume of the gas target, making TDSE-type calculations not very practical. Recently an alternative theoretical model has been proposed [21–23]. The model is based on the rescattering theory, and it is now called the QRS theory. A detailed discussion of the QRS for HHG from atoms or molecules is given in [35]. The QRS theory has accuracy comparable to the TDSE, but computationally it is much less demanding, close to the level of the SFA. According to the QRS, HHG yield can be expressed as

$$Y(\omega) \propto \omega^4 |W(E)|^2 |d(\omega)|^2, \quad (20)$$

where $d(\omega)$ is the photorecombination (PR) transition dipole matrix element and $W(E)$ describes the flux of the returning electrons, which is called the returning “wave packet”. The electron energy E is related to photon energy ω by the laser-free dispersion relation

$$E = \frac{p^2}{2} = \omega - I_p. \quad (21)$$

The validity of this model has been tested on rare-gas atoms and on H_2^+ [22,23]. Since the harmonic yield $Y(\omega)$ is proportional to $\omega^4 |x(\omega)|^2$, the dipole moment $x(\omega)$ induced by the laser field can be further written as

$$|x(\omega)| e^{i\phi(\omega)} = |W(E)| e^{i\eta(E)} |d(\omega)| e^{i\delta(\omega)}, \quad (22)$$

where $\phi(\omega)$ is the phase of the harmonic and $\eta(E)$ and $\delta(\omega)$ are the phase of the wave packet and the PR transition dipole moment, respectively. The PR transition dipole moment $d(\omega)$

is the property of target only and is independent of laser, while the energy dependent wave packet $W(E)$ is the property of the laser. Its magnitude depends on the ionization rate since the returning electrons are first released from the target by tunnel ionization. Under the same laser condition, different targets of the same I_p essentially give the same wave packet, except for an overall normalization due to the different tunneling rates. The QRS is a simple model that improves the SFA. It replaces the plane wave in the PR transition dipole moment in the SFA by the more realistic scattering wave. According to the QRS, the induced dipole moment is given by

$$x^{\text{QRS}}(\omega) = x^{\text{SFA}}(\omega) \frac{d^{\text{QRS}}(\omega)}{d^{\text{SFA}}(\omega)}, \quad (23)$$

where both $x^{\text{SFA}}(\omega)$ and $d^{\text{QRS}}(\omega)$ are complex numbers while $d^{\text{SFA}}(\omega)$ is either a pure real or pure imaginary number.

3. Model potential

Within the SAE approximation, single-atom response to the laser field can be obtained by solving the TDSE numerically. In our TDSE calculation, atomic potential takes the following form [34]:

$$V(r) = -\frac{Z_c + a_1 e^{-a_2 r} + a_3 r e^{-a_4 r} + a_5 e^{-a_6 r}}{r}, \quad (24)$$

where Z_c is the charge seen by the active electron asymptotically and a_1, \dots, a_6 are parameters obtained by fitting $V(r)$ to the numerical potential from self-interaction free density functional theory. Different forms of the model potential have been generated by others using different criteria. For example, a model potential for Ar was used by Muller [36] which gives the correct position of the Cooper minimum in the photoionization (or photorecombination) cross section. For each atom the same model potential is used in the TDSE and in the PR transition dipole moment calculations. In other words, the ground and the continuum state wave functions are calculated with the same model potential, which is also used in the TDSE. For such continuum wave functions, the scattering boundary conditions are imposed and thus they are called scattering waves. In [22,23], QRS theory is called the scattering-wave strong-field approximation (SW-SFA) model.

D. Wave packet extracted from macroscopic HHG

The validity of Eqs. (20) and (22) has been tested for the single-atom response to the laser field only so far. Since experimentally HHG is measured from a macroscopic medium, we examine whether a similar expression can be obtained. Specifically, we ask if the macroscopic HHG spectrum can be expressed as

$$S_h(\omega) \propto \omega^4 |W'(E)|^2 |d(\omega)|^2, \quad (25)$$

where $W'(E)$ is called MWP in order to distinguish it from the single-atom response and $d(\omega)$ is the PR transition dipole moment of single atom or molecule. In other words, after the macroscopic propagation, can one still extract the laser-

independent target structure from the HHG spectra?

In the following we will use PR transition dipole moment and PR differential cross section interchangeably. Note that they are related by a simple scaling factor

$$\frac{d\sigma}{d\Omega} \propto \frac{\omega^3}{p} |d(\omega)|^2, \quad (26)$$

where p is the momentum of the electron.

III. RESULTS AND DISCUSSION

A. Simulation parameters and photorecombination cross sections

In our numerical simulation, we take the fundamental laser pulse in space to be a Gaussian beam with cylindrical symmetry, propagating along the z direction. The beam waist at the laser focus is fixed as $w_0 = 25 \mu\text{m}$ and the confocal parameter b is given by $b = 2\pi w_0^2 / \lambda$, where λ is laser's central wavelength. A 1 mm long gas jet with constant atom density is placed after, at, or before the laser focus. In the time domain the laser pulse is assumed to have a cosine-squared envelope, and the carrier envelope phase is taken to be $\varphi_{CE} = 0$ rad. Equation (5) is solved for each frequency ω using the Crank-Nicholson method. Typical parameters used in the calculations are 300 grid points along the radial direction and 400 grid points along the longitudinal direction.

In Fig. 1, we plot photorecombination cross sections (PRCSs) in terms of photon energy for Ar, Xe, and Ne. For each target, we first show the “exact” PRCS where the ground state and continuum state wave functions are obtained “exactly” from the model potential, i.e., the continuum electron is represented by the scattering wave. In the second model, the same ground state wave function is used, but plane wave is used for the continuum state. In the third model, the target atom is replaced by an effective “hydrogenlike” atom where the nuclear charge is chosen such that its $1s$ binding energy is the same as the binding energy of the target atom. In this calculation, the final state is still described by a plane wave, i.e., only the initial wave function is different from the second model. Note that in the examples used, the ground state of each target atom has p -orbital symmetry, while in the hydrogenlike target, it has the s -orbital symmetry. There are a number of distinct features from these results that deserve discussion. First, the exact PRCSs for three targets are distinctly different. For Ar, there is a Cooper minimum occurring near 42 eV (if the model potential of Muller [36] is used the minimum occurs near 50 eV; see [35]). For Ne there is no such minimum (the general rule for the existence of Cooper minimum has been given long time ago [37]). Using the second model, the PRCS shows a minimum for each atom, and it is the recombination matrix element used in the SFA. In the third model, the dipole matrix element is given by the analytical formula of Eq. (19). The PRCS calculated using this model is monotonically decreasing after it reaches a maximum very near the ionization threshold.

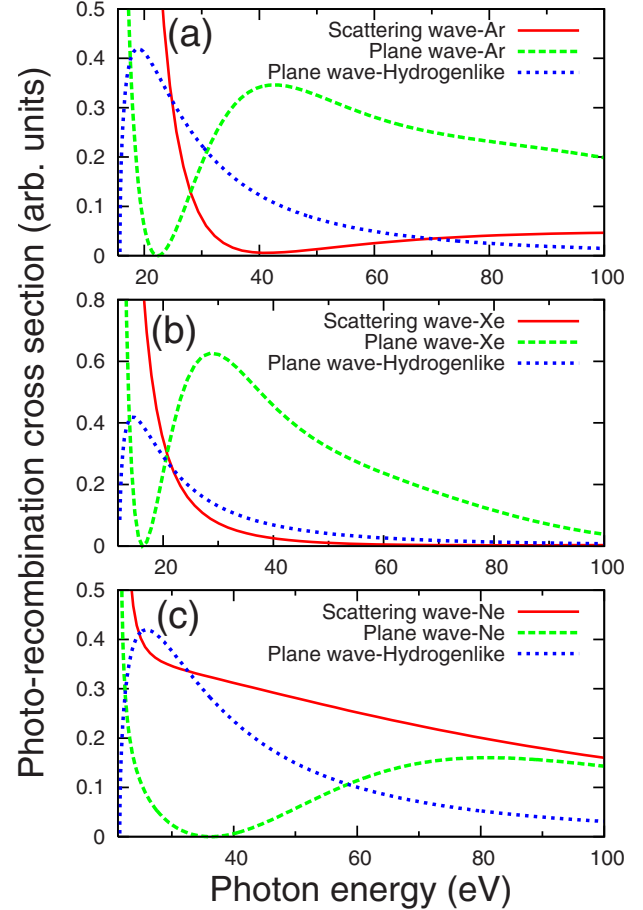


FIG. 1. (Color online) Photorecombination cross sections of (a) Ar, (b) Xe, and (c) Ne, obtained by using scattering wave (solid lines) and within plane wave approximation using real atom (dashed lines) and hydrogenlike atom (dotted lines).

B. Macroscopic HHG spectra: QRS vs TDSE

1. Strength of the harmonics

With the amplitude and phase of single-atom HHG calculated from the TDSE, SFA, and QRS as the source terms for the macroscopic propagation equations, we calculated and compared the macroscopic HHG spectra from these three different models.

In Fig. 2(a), single-atom HHG spectra of Ar exposed to a 19.4 fs (FWHM) laser pulse with peak intensity of $1.5 \times 10^{14} \text{ W/cm}^2$ and central wavelength of 800 nm are shown. The spectra from the QRS and SFA are normalized to that from the TDSE near the cutoff, i.e., close to $(I_p + 3.2U_p) / \omega_0$ [18,38], where U_p is ponderomotive energy. The QRS model is a substitute for the SFA, which can be easily carried out by Eq. (23). We can see that HHG spectra in the plateau region are very noisy, with no clear peaks at odd harmonics except in the cutoff region. It also shows that the SFA agrees with the TDSE only for harmonics close to the cutoff, while in the plateau region there are large discrepancies. For the QRS, on the other hand, there is a good agreement with the TDSE except for a sharp spike near harmonic 14 (or H14). The abnormal spike near H14 can be easily traced to zero of the PRCS in the plane wave approxi-

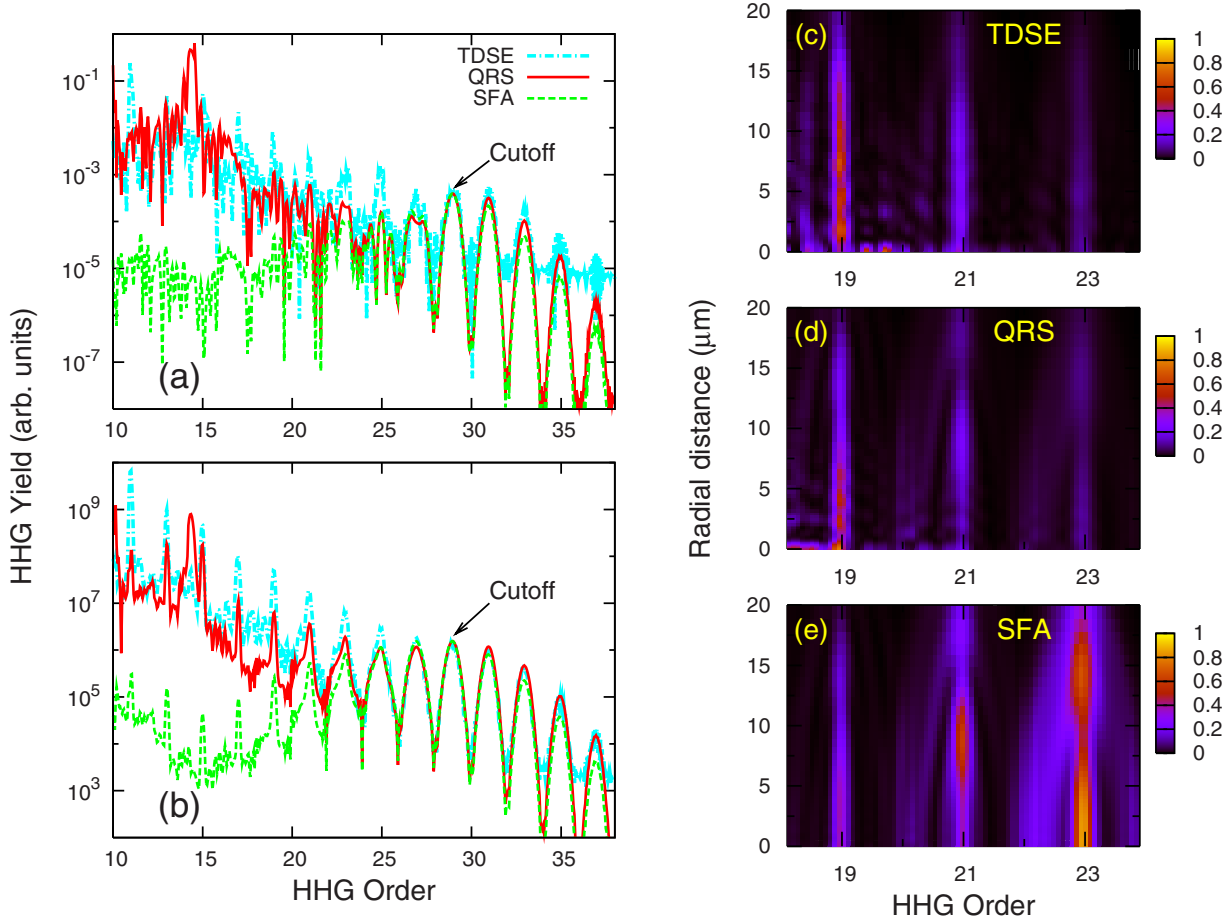


FIG. 2. (Color online) (a) Single atom and (b) macroscopic harmonic spectra of Ar from the TDSE (dot dashed lines), QRS (solid lines), and SFA (dashed lines). Spatial distribution of macroscopic harmonic emission at the exit face of gas jet from the (c) TDSE, (d) QRS, and (e) SFA.

mation shown in Fig. 1(a). This single-atom response result has been studied extensively in Le *et al.* [22].

In Fig. 2(b), we show the macroscopic HHG spectra of Ar when gas jet is placed 2 mm after the focus and laser peak intensity at the center of the gas jet is $1.5 \times 10^{14} \text{ W/cm}^2$. The pulse duration and wavelength are the same as in Fig. 2(a). Three different atomic dipoles from the TDSE, QRS, and SFA are applied to calculate the source term in Eq. (5). The HHG signal at the exit after propagation is collected using Eq. (8). The HHG spectra after propagation from the QRS and the SFA are again normalized to that from TDSE in the cutoff region. Several general features of the macroscopic HHG spectra are clear: sharp drop of the spectra beyond the cutoff; well-resolved odd harmonics are observed across the whole plateau; spectral widths are smaller in the plateau and increase with the harmonic order; and the cutoff location of the spectrum is around $(I_p + 3.2U_p)/\omega_0$ as in single-atom response. In comparison with single-atom HHG spectrum in Fig. 2(a), the propagation cleans up the spectra between odd harmonics. The relative intensity of odd harmonics does not change too much even after propagation. If we only look at the cutoff region, the SFA gives correct prediction with the TDSE. Obviously, it fails for the lower plateau spectrum. The QRS model, after the propagation, gives a much closer agreement with the one obtained from

the TDSE over the whole spectral region. This result shows that the QRS is capable of improving the SFA quite significantly, but with computational effort close to the SFA. Again the spike in the propagated spectra near H14 is caused by the same reason as in the single-atom case.

At this point we want to note that an approximate propagated spectrum from the QRS can be obtained directly from the propagated SFA spectrum. In fact, under the weak ionization condition, the polarization $\tilde{P}_{nl}(r, z', \omega) \propto x(r, z', \omega)$. Due to the factorization of the induced dipole in the QRS [see Eq. (23)], the source term in Eq. (5) for the QRS is different from that of the SFA by an overall factor of $d^{\text{QRS}}(\omega)/d^{\text{SFA}}(\omega)$. This results in the same overall factor for $\tilde{E}_h(r, z', \omega)$ from the QRS as compared to the SFA. The above is not expected to hold for general cases, for example, when the absorption of the HHG during the propagation is significant.

In Fig. 2(b), only the total HHG signal at the exit face of gas jet has been displayed. An interesting question is how the QRS model improves over the SFA in comparison with the TDSE for the harmonic field intensity in different regions of the exit face (which has cylindrical symmetry). In Figs. 2(c)–2(e), the strength $|\tilde{E}_h(r, z', \omega)|^2$ vs the radial distances for H19–H23 are shown based on the three models. Again, the TDSE and the QRS show good overall agreement. This

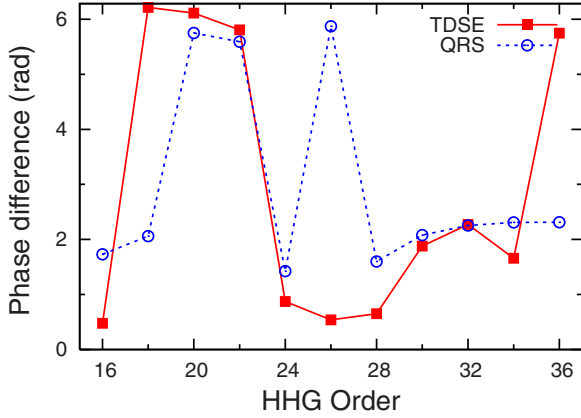


FIG. 3. (Color online) Phase difference $\Delta\phi$ of single-atom response for Ar from the TDSE (solid squares) and QRS (open circles).

comparison also offers a good reason for adopting QRS-based single-atom response for the macroscopic propagation of HHG.

2. Phase of the harmonics

The phase of HHG is crucial for attosecond pulse generation. According to Eq. (22), the phase of harmonics gets contribution from the returning wave packet, as well as from the complex PR transition dipole moment. How is the harmonic phase affected by the macroscopic propagation? This question also demands a proper way to present the phase of harmonics. According to semiclassical theory, the phase difference between successive odd harmonics reveals the harmonic emission time [39]. Since the phase difference between consecutive odd harmonics can be measured using the reconstruction of attosecond beating by interference of two-photon transition (RABITT) technique [40,41] experimentally, we choose to study the phase difference as defined by

$$\Delta\phi_{2n} = \phi_{2n+1} - \phi_{2n-1}. \quad (27)$$

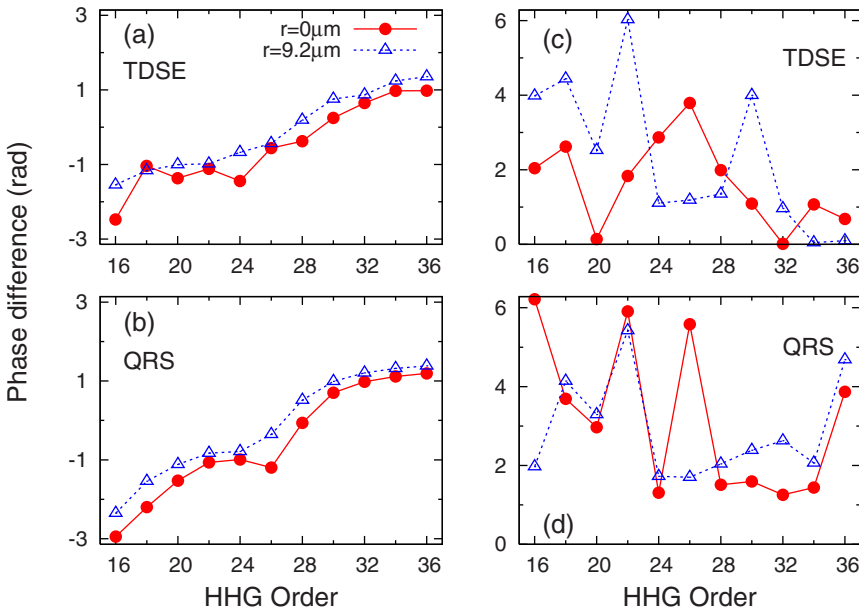


FIG. 4. (Color online) Phase difference $\Delta\phi$ of macroscopic response for Ar from the TDSE and the QRS, which is calculated for $r=0 \mu\text{m}$ (solid circles) or $r=9.2 \mu\text{m}$ (open triangles) at the exit of gas jet. [(a) and (b)] Gas jet is put 2 mm after the focus. [(c) and (d)] Gas jet is put at the focus. The laser intensity in the center of gas jet is always kept as $1.5 \times 10^{14} \text{ W/cm}^2$; laser duration and wavelength are the same as in Fig. 2.

In Fig. 3, we show the phase difference for single-atom response of Ar from the TDSE and the QRS for the same laser parameters used to obtain Fig. 2(a). The phase difference is shown in the interval $[0, 2\pi]$. In the plateau region, both the TDSE and the QRS give irregular phase differences, but the phases are locked in the cutoff region. In Figs. 4(a) and 4(b), we show the phase difference of macroscopic response for Ar from TDSE and QRS, where the spectral strength has been shown in Fig. 2(b). Define the phase difference in the interval $[-\pi, \pi]$, we show the successive phase difference at two different positions $r=0 \mu\text{m}$ and $r=9.2 \mu\text{m}$ at the exit face of gas jet. Since harmonic fields emitted at different radial positions finally are added up incoherently when a few odd harmonics are combined to generate attosecond pulse [42,43], it is meaningful to observe phase behavior of harmonics in different positions separately. From Fig. 4(a) the phase difference increases almost linearly with the harmonic order (linear chirp [39]) with the same slope for both $r=0 \mu\text{m}$ and $r=9.2 \mu\text{m}$ due to phase matching, but the curve for $r=9.2 \mu\text{m}$ is shifted up in comparison with $r=0 \mu\text{m}$. In these two cases the absolute phase increases quadratically with the harmonic order. In Fig. 4(b), the QRS gives the same phase behavior as the TDSE in Fig. 4(a). Again, this shows the validity of the QRS in studying the macroscopic response.

In order to understand the mechanism of HHG phase behavior after the propagation, we move the gas jet into the laser focus, fix the laser peak intensity at its center to be $1.5 \times 10^{14} \text{ W/cm}^2$, and keep other laser parameters the same as in Figs. 4(a) and 4(b). Phase differences of macroscopic response for Ar from TDSE and QRS are shown in Figs. 4(c) and 4(d). Whether $r=0 \mu\text{m}$ or $r=9.2 \mu\text{m}$, both the TDSE and the QRS give randomlike phase differences and are similar to single-atom response in Fig. 3. Note that our observation of this phase behavior agrees with TDSE calculation of Gaarde and Schafer [43] (see their Fig. 3).

3. Semiclassical model of short and long electron trajectories

The processes that lead to single-atom HHG can be understood using the concept of Feynman's path integrals [20,44], which correspond to complex trajectories (quantum paths) followed by the electrons from the moment of ionization to the end of recombination with the parent ion, after having been accelerated in the driving ir field [45]. The electrons that give the most relevant contribution to the harmonics in the plateau region follow either short or long trajectories, respectively, characterized by travel time in the continuum close to one half or to a full optical period. Based on the saddle-point approximation, single-atom dipole response can be written as [46–49]

$$x(\omega) = \sum_{\text{short}} x_s(\omega) e^{i\Phi_s(\omega)} + \sum_{\text{long}} x_\ell(\omega) e^{i\Phi_\ell(\omega)}. \quad (28)$$

The first coherent sum in Eq. (28) is over the short trajectories, while the second coherent sum is over the long trajectories. In general, the phase from the short trajectories has a weaker dependence on laser intensity, while for the long trajectories the dependence is much stronger [50]. For single-atom response, contributions from both short and long trajectories interfere in the plateau region, leading to complex irregular peaks seen in Fig. 2(a) and random phase differences in Fig. 3. Near the cutoff, two trajectories merge into one, thus well-resolved odd harmonics appear in Fig. 2(a), and the phase difference becomes more regular (see Fig. 3).

When macroscopic propagation is considered the induced dipoles from individual atoms interfere. The interference tends to wash out contributions from long trajectories because their phases Φ_ℓ have stronger laser intensity dependence. However, the geometric phase of the fundamental field also contributes to the interference. When the gas jet is placed after the laser focus, the geometric phase tends to cancel out the phase of the induced atomic dipole [see Eq. (15)], thus resulting in well-resolved odd harmonics seen in Fig. 2(b). If the gas jet is placed at the laser focus (or before the focus), the geometric phase is added to atomic dipole phase. The lack of phase cancellation leads to irregular harmonics strength and phases, similar to the single-atom case. Note that the major consequence of macroscopic propagation considered here is due to the phase-matching condition.

Since single-atom dipole phase is predominantly determined by the laser field which is adequately described by the SFA, phase-matching condition is nearly the same whether one uses SFA, QRS, or TDSE to calculate the single-atom response. This explains why propagation calculations using SFA-based atomic dipoles have been so successful in explaining many features of macroscopic HHG, especially the temporal profiles of the synthesized attosecond pulses. By using the QRS or the TDSE, a small and nearly energy-independent phase is added to the phase of each harmonic (except in region where the phase of the recombination dipole changes rapidly like near the Cooper minimum). The major differences between the QRS-based (or TDSE) and the SFA-based atomic dipoles are the relative strength (i.e., the amplitude) of different harmonic orders. When superposing these harmonics, it is well known that the relative phase of

the harmonics is much more important than the amplitude in determining the temporal profile of the resulting attosecond pulses, and for this purpose the SFA-based model is quite adequate.

C. MWP

Having established the validity of calculating macroscopic response of HHG using QRS-based atomic dipoles, we now proceed to investigate our second goal: can one extract the atomic PR dipole moment from the macroscopic HHG spectra? We answer this question in a different way. Taking Ar target as an example, we can use the QRS to generate single-atom induced dipole moment and then carry out the propagation to obtain the macroscopic HHG. Recall that in this case the single-atom wave packet is calculated from SFA using the ground state wave function of Ar, and the MWP $W'(\omega)$ has been defined in Eq. (25). Using laser parameters and focusing condition the same as those for Fig. 2(b), we show the resulting MWP in Fig. 5(a). In this figure, we also show another MWP calculated from a hydrogenlike system where the effective nuclear charge has been adjusted such that its $1s$ binding energy is the same as the $3p$ ground state energy of Ar. By normalizing the two MWPs at the cutoff energy (marked by an arrow and estimated from the peak intensity of the gas center) we see that they agree relatively well. The agreement gets better as laser intensity decreases. This is shown in Fig. 5(b), where the laser peak intensity in the center of gas jet is reduced to 1.25×10^{14} W/cm². This shows that MWP is mostly determined by the laser parameters and focusing condition, and we can take the MWP to be independent of the targets. The agreement is reflected even in the case when good phase matching is not met [see Fig. 5(c)], where the laser peak intensity in the center of gas jet is kept at 1.5×10^{14} W/cm², but the gas jet is put at 1.5 mm after the focus. Similar comparison has been carried out for Xe and Ne targets. In Fig. 5(d), the MWP is obtained from a laser pulse with duration of 21.8 fs, central wavelength of 1200 nm, and peak intensity of 5×10^{13} W/cm² in the center of the Xe gas jet, interacting with the gas jet setting at 2 mm after the focus. In Fig. 5(e), the MWP is obtained for a laser pulse with duration of 23.3 fs, central wavelength of 800 nm, and peak intensity of 2.5×10^{14} W/cm² at the Ne gas jet center, placed at 2.5 mm after the focus. These results indeed show that MWPs from different targets with same I_P agree with each other reasonably well under the same laser condition.

The above results are not surprising. As noted in Sec. III B, under the conditions and assumptions used in this paper, the macroscopic HHG yield can be factorized as the source term can be approximately factorized. This, however, is not expected to hold for general cases, for example, when the ionization or the absorption of the HHG by the medium is significant.

These results have important implications. Since atomic PR transition dipole is generally well known, by taking the HHG spectra of an atomic target and a molecular one with nearly identical binding energy in the same laser field, one can extract the transition dipole of the molecule. One can use

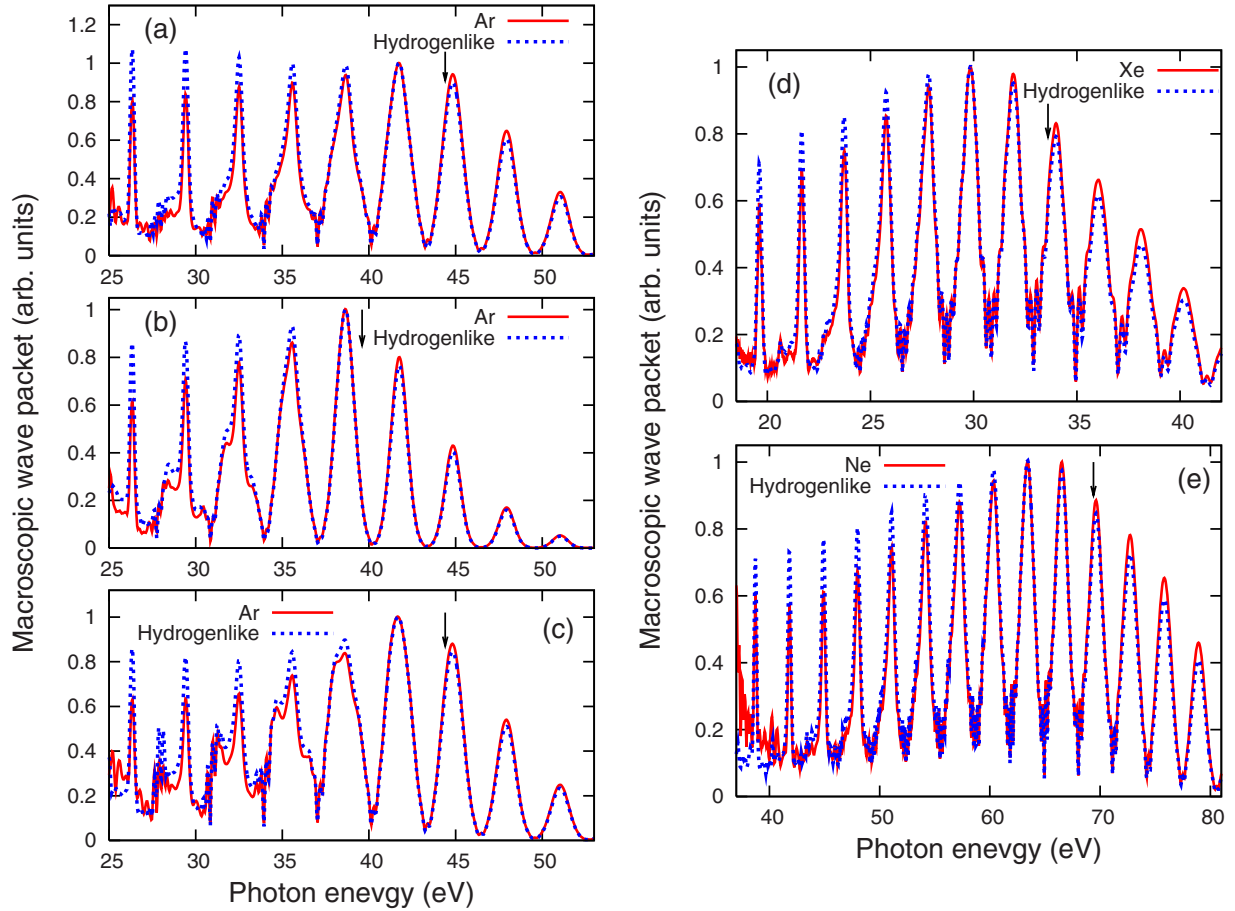


FIG. 5. (Color online) Macroscopic wave packet extracted from macroscopic harmonic spectrum based on QRS using real atom (solid lines) and hydrogenlike atom (dotted lines). [(a)–(c)] Ar gas jet is 2, 2, and 1.5 mm after the focus, respectively. Laser intensities are 1.5×10^{14} , 1.25×10^{14} , and 1.5×10^{14} W/cm², respectively. (d) Xe gas jet is 2 mm after the focus; laser intensity is 5×10^{13} W/cm². (e) Ne gas jet is 2.5 mm after the focus; laser intensity is 2.5×10^{14} W/cm². The arrows indicate the cutoff energy determined by $I_p + 3.2U_p$ [18,38]; laser intensity means one in the center of gas jet.

the same laser pulse to obtain HHG spectra for an unknown molecule and for a known atomic target with nearly the same binding energy. From the ratio of the HHG yields of the two targets and the known PR transition dipole of the atomic target, one can extract the transition dipole of the molecule. This model has been assumed by Itatani *et al.* [26] and by Levesque *et al.* [51]. Our results confirm the validity of their assumptions.

D. Phase-matching conditions

Phase matching plays an essential role in determining the efficiency of macroscopic HHG. From Eq. (15), atomic phase depends on the laser intensity [45] and it is separated from the geometric phase. Due to laser's focusing, both the atomic phase and geometric phase are varied in space. Since each individual harmonics has its own atomic phase dependence on laser intensity [48] and the harmonic order enters Eq. (15), thus phase-matching condition changes for different harmonic orders even at the same position [52,53].

It is instructive to examine how phase-matching leads to harmonic emission inside of a gas jet. In Fig. 6, we show evolution of harmonic intensities $|\tilde{E}_h(r, z', \omega)|^2$ (normalized)

in space for harmonics H15, H17, H25, and H27 obtained from the QRS. The laser parameters and gas jet position are the same as in Fig. 2(b). On the entrance plane at $z = 1.5$ mm, there is no harmonic field. As the induced harmonic field propagates along the z direction, the harmonic field for each order in space is enhanced or suppressed due to the different phase-matching condition. Finally, HHG signal is collected on the exit plane at $z = 2.5$ mm. From these figures, it is clear that it is difficult to reach best phase-matching condition for all the harmonics. But one can manipulate the gas jet position to obtain optimum harmonic yields.

E. Intensity averaging vs propagation effect

The above examples show that proper phase matching and spatial filtering during the macroscopic propagation are the keys to obtain enhanced odd high-order harmonics. Since solving the macroscopic propagation equation is still rather time consuming even with the simplification of using QRS-based atomic dipoles, it is of interest to check whether there are simpler methods that can obtain comparable results. According to Eq. (28) the induced atomic dipole can be sepa-

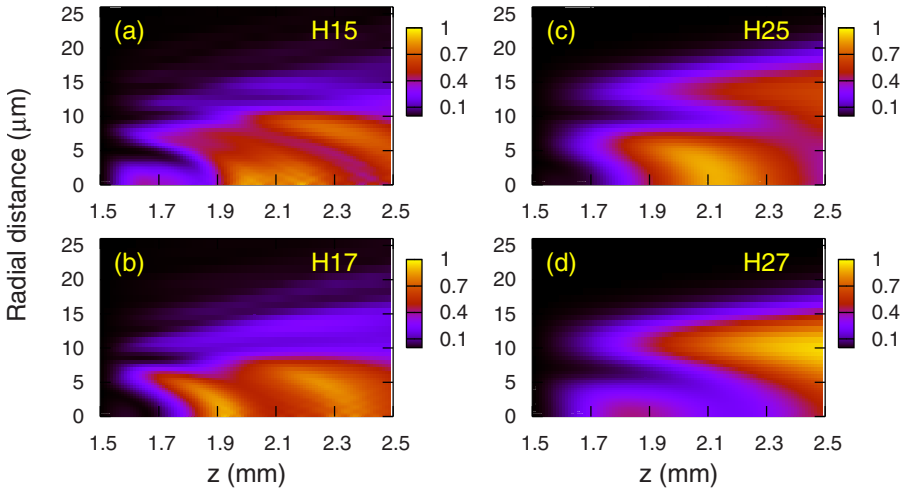


FIG. 6. (Color online) Spatially harmonic emission of (a) H15, (b) H17, (c) H25, and (d) H27 for Ar under the QRS.

rated into contributions from long and short trajectories, with the long-trajectory ones having phases that depend strongly on the laser’s intensity. Thus one way to achieve equivalent phase matching is to coherently summing up the induced single-atom dipoles for a proper range of laser intensity. This would have the effect similar to selecting the contributions from short trajectories only. Such a procedure is called “intensity averaging” and was used by Morishita *et al.* [21] and by Le *et al.* [22]. This method allows one to obtain reasonably looking regular odd HHG from the chaotically looking HHG generated from a single atom. It is mentioned that this selection is based purely on single-atom effect; there is no propagation involved.

How good is the intensity averaging procedure? In Figs. 7(a) and 7(b) we show HHG yields obtained from macroscopic propagation with single-atom induced dipoles calculated from the TDSE. The gas jets are placed 2 mm after the focus in Fig. 7(a) and 2 mm before the focus in Fig. 7(b); the other laser parameters are kept the same as in Fig. 2(b). Since the harmonics are most strongly emitted from region close to the z axis in general, for the intensity averaging

procedure we chose the intensity range to be the same as for the laser intensity range on the z axis in the gas jet. The result of this procedure is shown as the solid line in Fig. 7(a). One can see that intensity averaging agrees well with the propagated one in this case, where a good phase-matching condition is met. However this is not always the case in general. As an example we show in Fig. 7(b) the propagated HHG spectrum for gas jet placed 2 mm before the focus. It is clear that the result is different from the intensity averaged spectrum, as the latter is still the same as in Fig. 7(a). Similar tests have been carried out using the QRS-based atomic dipoles in Figs. 7(c) and 7(d). Note that harmonic intensities from H20 to H28 in Figs. 7(b) and 7(d) are multiplied by a factor of 6 in order to see their fine structures.

Our other tests indicate that up to about ten harmonics in the plateau region can be quite accurately simulated by the intensity averaging method when the gas jet is placed at the good phase-matching position. This is where the short trajectories are selected efficiently. When the gas jet is placed at other positions, the propagated HHG will still receive contributions from the long trajectories, whereas intensity averag-

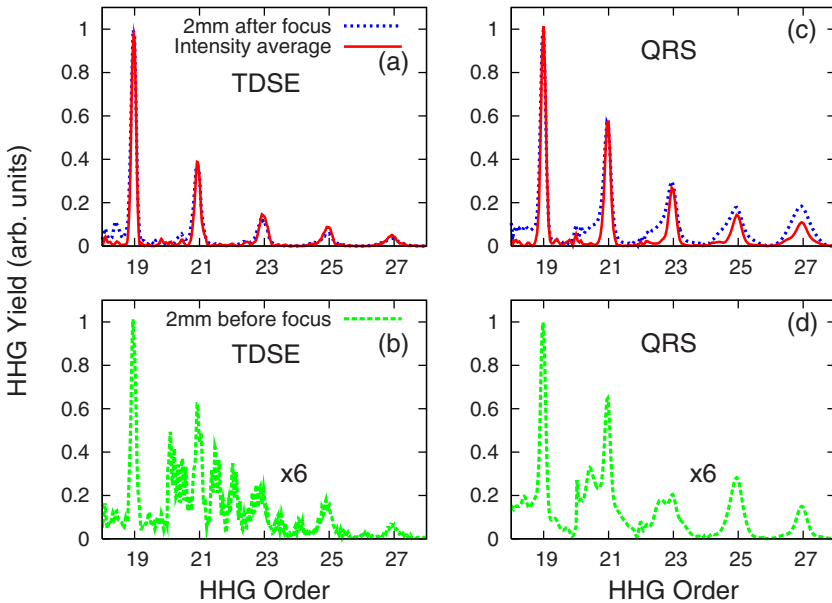


FIG. 7. (Color online) Intensity averaged harmonic spectra (solid lines) vs propagated one when gas jet is put 2 mm after (dotted lines) or before (dashed lines) the focus for Ar. (a) and (b) are shown the TDSE calculations; (c) and (d) are shown the QRS calculations. Harmonic yields of H20–H28 in (b) and (d) are multiplied by 6.

ing procedure essentially eliminates their contributions.

IV. SUMMARY AND OUTLOOK

In the past two decades HHG by intense ir laser pulses with atoms or molecules has been widely investigated both experimentally and theoretically. Since HHG is generated from a macroscopic medium, theoretical simulation usually consists of two parts. The first part is to obtain the microscopic induced dipole moment of each atom or molecule in the medium. The second part is the macroscopic propagation of Maxwell's equation. In this paper, first we showed that the induced atomic dipole moment calculated by recently developed QRS theory, which can be conveniently used to replace the one calculated by SFA. The resulting macroscopic HHG spectrum obtained from the QRS-based atomic dipoles is in much better agreement with the TDSE than that from the SFA.

In the macroscopic propagation we consider low intensity lasers and low density gas medium such that the effect of free electrons, the absorption, and dispersion of the medium can be neglected. Under such condition, we showed that macroscopic HHG spectra can be expressed as the product of a MWP and the single-atom photorecombination transition dipole moment, similar to the case for HHG by a single atom or molecule studied earlier. The MWP has been shown to be

largely independent of the target gas if the ionization potential is nearly the same for the two targets. This important result implies that one can extract the transition dipole of an unknown atom or molecule from one for which the transition dipole moment is known by comparing their measured HHG spectra in the same laser pulse. Since PR transition dipole moment is a property of atom or molecule, this means that measurement of macroscopic HHG spectra offers the opportunity to extract the structural information of molecules. More importantly, ir lasers of duration of a few femtoseconds are widely available already today. Using a typical pump and probe arrangement, one can use a pump laser to initiate a chemical reaction; the transient molecule can then be interrogated from the HHG spectra generated by a probe beam sent in at different delay times. In other words, the theoretical foundation for dynamic chemical imaging using high-order harmonics generated by ir lasers has been established. Its further progress will be its eventual experimental realization.

ACKNOWLEDGMENTS

We thank Mette B. Gaarde for the valuable discussions. This work was supported in part by Chemical Sciences, Geosciences and Biosciences Division, Office of Basic Energy Sciences, Office of Science, U.S. Department of Energy.

-
- [1] A. L'Huillier, D. Descamps, A. Johansson, J. Norin, J. Mauritsson, and C.-G. Wahlström, *Eur. Phys. J. D* **26**, 91 (2003).
- [2] C. Winterfeldt, C. Spielmann, and G. Gerber, *Rev. Mod. Phys.* **80**, 117 (2008).
- [3] T. Brabec and F. Krausz, *Rev. Mod. Phys.* **72**, 545 (2000).
- [4] F. Krausz and M. Ivanov, *Rev. Mod. Phys.* **81**, 163 (2009).
- [5] P. Agostini and L. F. DiMauro, *Rep. Prog. Phys.* **67**, 813 (2004).
- [6] P. Salières, A. L'Huillier, Ph. Antoine, and M. Lewenstein, *Adv. At., Mol., Opt. Phys.* **41**, 83 (1999).
- [7] Z. Chang, *Phys. Rev. A* **70**, 043802 (2004).
- [8] M. B. Gaarde, J. L. Tate, and K. J. Schafer, *J. Phys. B* **41**, 132001 (2008).
- [9] M. B. Gaarde, M. Murakami, and R. Kienberger, *Phys. Rev. A* **74**, 053401 (2006).
- [10] M. B. Gaarde, Ph. Antoine, A. L'Huillier, K. J. Schafer, and K. C. Kulander, *Phys. Rev. A* **57**, 4553 (1998).
- [11] M. B. Gaarde, F. Salin, E. Constant, Ph. Balcou, K. J. Schafer, K. C. Kulander, and A. L'Huillier, *Phys. Rev. A* **59**, 1367 (1999).
- [12] P. Salières, P. Antoine, A. de Bohan, and M. Lewenstein, *Phys. Rev. Lett.* **81**, 5544 (1998).
- [13] M. Bellini, C. Lyngå, A. Tozzi, M. B. Gaarde, T. W. Hänsch, A. L'Huillier, and C.-G. Wahlström, *Phys. Rev. Lett.* **81**, 297 (1998).
- [14] C. Lyngå, M. B. Gaarde, C. Delfin, M. Bellini, T. W. Hänsch, A. L'Huillier, and C.-G. Wahlström, *Phys. Rev. A* **60**, 4823 (1999).
- [15] C. Corsi, A. Pirri, E. Sali, A. Tortora, and M. Bellini, *Phys. Rev. Lett.* **97**, 023901 (2006).
- [16] S. X. Hu and L. A. Collins, *J. Phys. B* **39**, L185 (2006).
- [17] N. H. Shon, A. Suda, and K. Midorikawa, *Phys. Rev. A* **62**, 023801 (2000).
- [18] P. B. Corkum, *Phys. Rev. Lett.* **71**, 1994 (1993).
- [19] M. Lewenstein, Ph. Balcou, M. Yu. Ivanov, A. L'Huillier, and P. B. Corkum, *Phys. Rev. A* **49**, 2117 (1994).
- [20] M. B. Gaarde and K. J. Schafer, *Phys. Rev. A* **65**, 031406(R) (2002).
- [21] T. Morishita, A. T. Le, Z. Chen, and C. D. Lin, *Phys. Rev. Lett.* **100**, 013903 (2008).
- [22] A. T. Le, T. Morishita, and C. D. Lin, *Phys. Rev. A* **78**, 023814 (2008).
- [23] A. T. Le, R. D. Picca, P. D. Fainstein, D. A. Telnov, M. Lein, and C. D. Lin, *J. Phys. B* **41**, 081002 (2008).
- [24] V. H. Le, A. T. Le, R. H. Xie, and C. D. Lin, *Phys. Rev. A* **76**, 013414 (2007).
- [25] V. H. Le, N. T. Nguyen, C. Jin, A. T. Le, and C. D. Lin, *J. Phys. B* **41**, 085603 (2008).
- [26] J. Itatani, J. Levesque, D. Zeidler, H. Niikura, H. Pépin, J. C. Kieffer, P. B. Corkum, and D. M. Villeneuve, *Nature (London)* **432**, 867 (2004).
- [27] T. Kanai, S. Minemoto, and H. Sakai, *Nature (London)* **435**, 470 (2005).
- [28] C. Vozzi, F. Calegari, E. Benedetti, J.-P. Caumes, G. Sansone, S. Stagira, M. Nisoli, R. Torres, E. Heesel, N. Kajumba, J. P. Marangos, C. Altucci, and R. Velotta, *Phys. Rev. Lett.* **95**, 153902 (2005).
- [29] X. Zhou, R. Lock, W. Li, N. Wagner, M. M. Murnane, and H.

- C. Kapteyn, *Phys. Rev. Lett.* **100**, 073902 (2008).
- [30] W. Boutu, S. Haessler, H. Merdji, P. Breger, G. Waters, M. Stankiewicz, L. J. Frasinski, R. Taïeb, J. Caillat, A. Maquet, P. Monchicourt, B. Carre, and P. Salieres, *Nat. Phys.* **4**, 545 (2008).
- [31] E. Lorin, S. Chelkowski, and A. Bandrauk, *Comput. Phys. Commun.* **177**, 908 (2007).
- [32] E. Priori, G. Cerullo, M. Nisoli, S. Stagira, S. De Silvestri, P. Villoresi, L. Poletto, P. Ceccherini, C. Altucci, R. Bruzzese, and C. de Lisio, *Phys. Rev. A* **61**, 063801 (2000).
- [33] M. V. Ammosov, N. B. Delone, and V. P. Krainov, *Zh. Eksp. Teor. Fiz.* **91**, 2008 (1986) [*Sov. Phys. JETP* **64**, 1191 (1986)].
- [34] X. M. Tong and C. D. Lin, *J. Phys. B* **38**, 2593 (2005).
- [35] A. T. Le, R. R. Lucchese, S. Tonzani, T. Morishita, and C. D. Lin (unpublished); e-print arXiv:0903.5354.
- [36] H. G. Muller, *Phys. Rev. A* **60**, 1341 (1999).
- [37] J. W. Cooper, *Phys. Rev.* **128**, 681 (1962).
- [38] J. L. Krause, K. J. Schafer, and K. C. Kulander, *Phys. Rev. Lett.* **68**, 3535 (1992).
- [39] Y. Mairesse, A. de Bohan, L. J. Frasinski, H. Merdji, L. C. Dinu, P. Monchicourt, P. Breger, M. Kovačev, R. Taïeb, B. Carré, H. G. Muller, P. Agostini, and P. Salières, *Science* **302**, 1540 (2003).
- [40] P. M. Paul, E. S. Toma, P. Breger, G. Mullot, F. Augé, Ph. Balcou, H. G. Muller, and P. Agostini, *Science* **292**, 1689 (2001).
- [41] R. López-Martens, K. Varjú, P. Johnsson, J. Mauritsson, Y. Mairesse, P. Salières, M. B. Gaarde, K. J. Schafer, A. Persson, S. Svanberg, C.-G. Wahlström, and A. L’Huillier, *Phys. Rev. Lett.* **94**, 033001 (2005).
- [42] Ph. Antoine, A. L’Huillier, and M. Lewenstein, *Phys. Rev. Lett.* **77**, 1234 (1996).
- [43] M. B. Gaarde and K. J. Schafer, *Phys. Rev. Lett.* **89**, 213901 (2002).
- [44] P. Salières, B. Carré, L. Le Déroff, F. Grasbon, G. G. Paulus, H. Walther, R. Kopold, W. Becker, D. B. Milošević, A. Sanpera, and M. Lewenstein, *Science* **292**, 902 (2001).
- [45] M. Lewenstein, P. Salières, and A. L’Huillier, *Phys. Rev. A* **52**, 4747 (1995).
- [46] G. Sansone, C. Vozzi, S. Stagira, M. Pascolini, L. Poletto, P. Villoresi, G. Tondello, S. De Silvestri, and M. Nisoli, *Phys. Rev. Lett.* **92**, 113904 (2004).
- [47] G. Sansone, E. Benedetti, J.-P. Caumes, S. Stagira, C. Vozzi, S. De Silvestri, and M. Nisoli, *Phys. Rev. A* **73**, 053408 (2006).
- [48] G. Sansone, C. Vozzi, S. Stagira, and M. Nisoli, *Phys. Rev. A* **70**, 013411 (2004).
- [49] E. Benedetti, J.-P. Caumes, G. Sansone, S. Stagira, C. Vozzi, and M. Nisoli, *Opt. Express* **14**, 2242 (2006).
- [50] F. Lindner, W. Stremme, M. G. Schätzel, F. Grasbon, G. G. Paulus, H. Walther, R. Hartmann, and L. Strüder, *Phys. Rev. A* **68**, 013814 (2003).
- [51] J. Levesque, D. Zeidler, J. P. Marangos, P. B. Corkum, and D. M. Villeneuve, *Phys. Rev. Lett.* **98**, 183903 (2007).
- [52] Ph. Balcou, P. Salières, A. L’Huillier, and M. Lewenstein, *Phys. Rev. A* **55**, 3204 (1997).
- [53] L. E. Chipperfield, P. L. Knight, J. W. G. Tisch, and J. P. Marangos, *Opt. Commun.* **264**, 494 (2006).